Subwavelength plasmonic cavity resonator on a nanowire with periodic permittivity variation

Jingjing Li* and Nader Engheta†
Department of Electrical and Systems Engineering, University of Pennsylvania, Philadelphia, Pennsylvania 19104, USA
(Received 3 February 2006; revised manuscript received 16 July 2006; published 27 September 2006)

An electromagnetic cavity resonator with deep subwavelength size is considered theoretically on plasmonic nanowires with periodically modulated permittivity. In this work, plasmonic nanowires are treated as ϵ-negative cylindrical waveguides (ENGCWs) in a certain band of frequency whose guided wavelength for a small radius waveguide is small compared to the free-space wavelength. The dispersion relations of an ENGCW with permittivity varied periodically along the axial direction are then studied analytically using the space harmonic method and evanescent modes near the center of the band gap are analyzed in detail. By properly creating a "defect" on such a periodically modulated (PM) ENGCW, a cavity on this nanowire can be synthesized whose dimension along the wire is determined by the guided wavelength and the decay rate of the evanescent mode, resulting in an ultracompact subwavelength cavity resonator with a size much smaller than the free-space wavelength. The effective size of this cavity is calculated numerically. The finite-element method (FEM) is used to simulate the reflection phenomena at the interface of ENGCW/PMENGCW and to demonstrate the cavity mode. The quality factor (Q) is discussed and calculated from the FEM results. Candidate materials suitable for making this structure are suggested. A method to realize such a resonating structure using only one material is also briefly analyzed. Finally, a few words about the lower limit of such nanowires are given.

DOI: 10.1103/PhysRevB.74.115125 PACS number(s): 42.25.Bs, 42.70.Qs, 73.20.Mf

I. INTRODUCTION

Plasmonic materials, and the devices and structures that are made out of them, have been under intensive study in recent years.[1] Their ability to interact with optical signals within concentrated small regions provides exciting possibilities for manipulating optical information at dimensions far smaller than the free-space wavelength.[2,3] With the development of nanotechnology and the availability of various nanofabrication techniques, it is now possible to construct nanoscale subwavelength structures and devices from plasmonic materials that can exhibit exciting characteristics in the optical frequencies.[4,5] Components and elements such as plasmonic waveguides,[6,7] optical nanoantennas,[8] superlenses,[9,10] wire resonators,[11] and nanocircuit elements[12] have been investigated.

Photonic-band-gap (PBG) structures or photonic crystals (PCs), were first introduced as a method to inhibit spontaneous emission,[13] but over the years they have been shown to contribute to many other applications.[14,15] PCs are usually made of periodic arrangements of metallic or dielectric inhomogeneities with periodicities that are comparable to half of the wavelength of operation. Periodical structures made of plasmonic materials have also been reported, such as gratings[16] and subwavelength photonic crystals.[17]

One of the basic structures in electromagnetic systems is the cavity resonator, which is a building block in the design of various components and devices such as filters, Fabry-Pérot resonators, lasers, oscillators, etc. Reducing the size of cavity resonators has been a problem of great interest over the years. Various ideas and methods have been suggested. For example, defect modes in PBG structures are designed where the optical energy can be confined to the defect surrounded by a PC when operated in the band gap.[15,18,19] By this method the smallest cavity mode volume realized is $(\lambda_0/n)^3$, or approximately λ_0/n in each dimension, where λ_0 is the free-space wavelength and n is the refractive index of the material.[18] Use of double-negative or single-negative metamaterials to reduce the size of the resonator has also been suggested. Pairing them with double-positive or any materials with oppositely signed parameters can achieve phase compensation which leads to subwavelength cavity resonators.[20–22]

In this paper, we suggest and analyze another method to achieve cavity resonators whose volumes can be much smaller than the traditional value of $(\lambda_0/n)^3$. In this approach, we exploit the slow-wave nature of guided waves along the cylindrical plasmonic nanowires due to the negative permittivity (ϵ negative) of the material, and we combine this feature with the defect mode of a periodic structure along such nanowires. The plasmonic nanowire is used as a negative-permittivity cylindrical waveguide whose permittivity is periodically modulated along the axial direction. With an azimuthally symmetric mode distribution, such a structure can be viewed as a one-dimensional (1D) PC on a plasmonic nanowire. When the waveguide diameter decreases, it is well known that the guided wavelength λ_g decreases. Also, we can show that the decaying constant for the evanescent mode on such a 1D PC actually increases as the diameter decreases, so that a defect mode introduced on it can have very small size.

The paper is organized as follows. In Sec. II the dispersion relations of guided modes on an ϵ-negative cylindrical waveguide (ENGCW) are briefly reviewed and their features are compared with those of the conventional positive-ϵ cylindrical waveguides. Section III discusses the dispersion relations of periodically modulated (PM) ENGCWs and various dispersion diagrams for both propagating and evanescent modes are given. The defect mode in a PMENGCW is discussed and the dimension of the minimum resonating mode

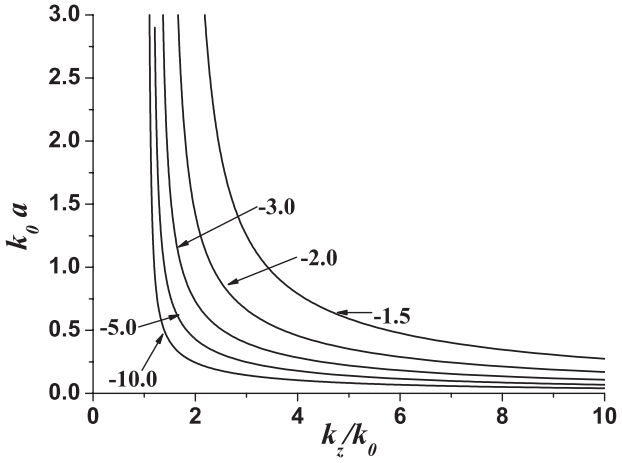

FIG. 1. Normalized radius vs normalized propagation constant (normalized to k_0) for ENGCWs of different ϵ_r at fixed frequency.

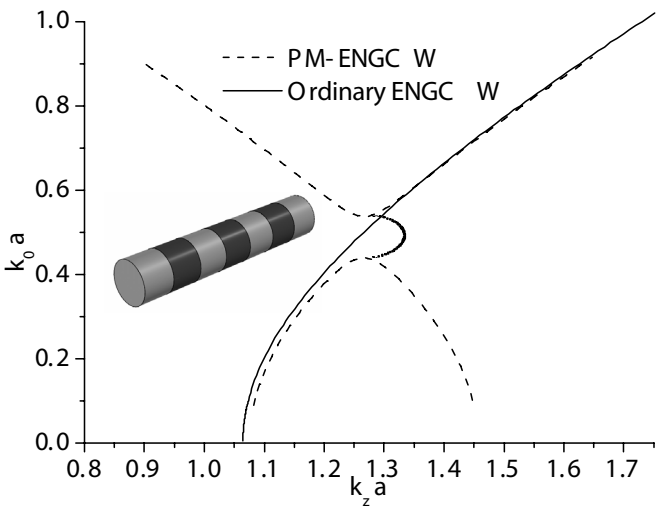

FIG. 2. Normalized frequency vs normalized propagation constant (normalized to radius a) for PMENGCW of $\epsilon_{ra}=-3.0$, $\Lambda=10\%$. In this plot, it is assumed that the permittivities are independent of frequencies. Inset: 3D plot of the model.

is evaluated in Sec. IV. The quality factor of such an ultracompact subwavelength resonating mode is also addressed. Section V gives the finite-element method (FEM) simulation results for the evanescent mode and the ultracompact cavity modes. Further discussions on realizing permittivity modulation and the quantum limit are given in Sec. VI and conclusions are in Sec. VII.

II. DISPERSION RELATION OF THE ENGCW

It is useful to review the dispersion relation of cylindrical waveguides, of both positive and negative permittivities. Since for the plasmonic nanowire the surface plasmon polariton is equivalent to the lowest-order transverse magnetic (TM01) mode, here only the TM01 modes of cylindrical waveguides are studied. The dispersion characteristics of the TM01 mode for the ϵ-positive cylindrical waveguide of relative permittivity ϵ_r are well known, and the main features are emphasized here. The propagating constant k_z satisfies $k_0 < k_z < \sqrt{\epsilon_r} k_0$, where k_0 is the free-space wavenumber. As the diameter of the waveguide decreases, k_z decreases, approaching k_0 and the mode becomes more weakly bound to the waveguide until it is cut off at a certain diameter. The ENGCW shows a great difference, as in Fig. 1. For a fixed frequency, the propagating constant k_z is always bigger than k_0, and will increase dramatically as the diameter decreases approaching zero. This means no cutoff of TM01 will happen and a guided wavelength $\lambda_g = 2\pi/k_z$ much smaller than the free-space wavelength can be achieved at small waveguide diameter. The mode cross section also decreases dramatically as diameter decreases. In other words, the mode becomes more tightly bound at smaller diameter. Dispersion relations for different values of negative permittivity are shown in Fig. 1. For the same normalized radius $k_0 a$, a smaller magnitude of negative ϵ_r gives a higher wave number k_z. Also, at small magnitude ϵ_r, change of ϵ_r for the same magnitude will have a more profound influence on the dispersion relation compared to the case at high magnitude of negative ϵ_r. This can be seen from the fact that the dispersion curves are "denser" at the high-$|\epsilon_r|$ side in Fig. 1, even though the $|\epsilon_r|$ differences between each two neighboring curves are bigger at the high-$|\epsilon_r|$ side than that of the low-$|\epsilon_r|$ side. These characteristics will have an important influence on the problems discussed later.

III. DISPERSION RELATION OF THE PMENGCW

Considering a PMENGCW with radius a and relative permittivity as a function of z given by (see the inset in Fig. 2)

$$\epsilon_r(z) = \begin{cases} \epsilon_{r\ \mathrm{low}} = \epsilon_{ra} + \epsilon_{rm}, & nd < z < \left(n + \frac{1}{2}\right)d, \\ \epsilon_{r\ \mathrm{high}} = \epsilon_{ra} - \epsilon_{rm}, & \left(n + \frac{1}{2}\right)d < z < (n+1)d, \end{cases} \tag{1}$$

where n is an integer, ϵ_{rm} the modulation magnitude, $\epsilon_{ra} < 0$ the average permittivity, $0 < \epsilon_{rm} < |\epsilon_{ra}|$, and d the modulation period. The subscripts "high" and "low" indicate high or low magnitude of the permittivity. The device is put in free space of permittivity ϵ_0. The analytical approach is similar to the treatment in the work of Peng *et al.*,[23] where planar periodic structures were discussed. From Maxwell's functions it is easy to see that for the TM01 mode, the magnetic field inside the waveguide can be constructed from

$$H_{\phi d} = \epsilon_r^{1/2} F(z) \tag{2}$$

where $F(z)$ is an auxiliary function satisfying

$$\left(\frac{\partial^2}{\partial \rho^2} + \frac{1}{\rho}\frac{\partial}{\partial \rho} - \frac{1}{\rho^2} + \frac{\partial^2}{\partial z^2}\right)F + k_F^2(z)F = 0, \tag{3}$$

$$k_F^2(z) = k_0^2 \epsilon_r(z) - \frac{3}{4}\left(\frac{\epsilon_r'(z)}{\epsilon_r(z)}\right) + \frac{1}{2}\left(\frac{\epsilon_r''(z)}{\epsilon_r(z)}\right) \tag{4}$$

where k_0 is the free-space wave number, and $\epsilon_r'(z)$ and $\epsilon_r''(z)$ the first and second derivatives of $\epsilon_r(z)$ with respect to z,

respectively. $k_F(z)$ is the "effective wave number" for the auxiliary field F. Because $\epsilon_r(z)$ is periodic, $k_F(z)$ is also periodic and can be generally represented by a Fourier series as

$$k_F^2(z) = k_0^2 \sum_n p_n \exp\left(in\frac{2\pi}{d}z\right). \tag{5}$$

Guess a solution of the form (using the $e^{-i\omega t}$ convention)

$$F = \sum_n q_n(\rho)\exp(ik_{z0}z)\exp\left(in\frac{2\pi}{d}z\right). \tag{6}$$

Inserting Eq. (6) into Eq. (3), by balancing the coefficient of each space harmonic we get

$$\left(\frac{\partial^2}{\partial\rho^2} + \frac{1}{\rho}\frac{\partial}{\partial\rho} - \frac{1}{\rho^2} + \frac{\partial^2}{\partial z^2}\right)\boldsymbol{q} = -\boldsymbol{P}\boldsymbol{q}, \tag{7}$$

where $\boldsymbol{q}=\boldsymbol{q}(\rho)$ is a column vector of components $q_n(\rho)$ and $\boldsymbol{P}$ a matrix whose elements are independent of ρ as $P_{nl} = k_0^2 p_{n-l} - k_{zn}^2 \delta_{nl}$ with δ_{nl} the Kronecker delta. Equation (7) is a group of differential equations for $q_n(\rho)$ coupled together through the matrix $\boldsymbol{P}$. Observing the form of Eq. (7) we try a solution as

$$\boldsymbol{q} = \boldsymbol{c}J_1(\beta\rho) \tag{8}$$

where β_ρ is a constant to be determined while $\boldsymbol{c}$ is a constant vector (independent of ρ) related to β_ρ. J_1 is the Bessel function of the first kind and of order 1. Inserting Eq. (8) into Eq. (7) we have

$$\boldsymbol{P}\boldsymbol{c} = \beta_\rho^2 \boldsymbol{c}. \tag{9}$$

Thus β_ρ^2 is an eigenvalue of $\boldsymbol{P}$ and $\boldsymbol{c}$ is the corresponding eigenvector. For the mth eigenvalue and eigenvector ($\beta_{\rho m}^2$, $\boldsymbol{c}_m$) the corresponding solution for the vector $\boldsymbol{q}$ is

$$\boldsymbol{q}_m = \boldsymbol{c}_m J_1(\beta_{\rho m}\rho). \tag{10}$$

Combining Eqs. (1), (6), and (10) we get for $\rho < a$

$$H_{\phi d} = \sum_{n,m,l} g_m c_{lm} J_1(\beta_{\rho m}\rho) r_{n-l} \exp(ik_{zn}z),$$

$$E_{zd} = \frac{i}{\omega\epsilon_0}\sum_{n,m,l} \beta_{\rho m} g_m c_{lm} J_0(\beta_{\rho m}\rho) w_{n-l} \exp(ik_{zn}z), \tag{11}$$

where $k_{zn}=k_{z0}+n2\pi/d$ with k_{z0} to be determined by boundary conditions, r_n are the Fourier coefficients of $\epsilon_r^{1/2}(z)$ while w_n the Fourier coefficient of $\epsilon_r^{-1/2}(z)$. c_{lm} are the lth components of the mth eigenvector $\boldsymbol{c}_m$. g_m are linear combination coefficients of $\boldsymbol{q}_m$. For $\rho > a$, the field distribution can be written as

$$H_{\phi 0} = \sum_n h_n K_1(\alpha_n\rho)\exp(ik_{zn}z),$$

$$E_{z0} = \frac{i}{\omega\epsilon_0}\sum_n \alpha_n h_n K_0(\alpha_n\rho)\exp(ik_{zn}z), \tag{12}$$

where α_n satisfies $k_{zn}^2 - \alpha_n^2 = k_0^2$. K_1 and K_0 are modified Bessel functions of the second kind of order 1 and 0, respectively and h_n are coefficients of the linear combination. By satisfying the boundary conditions and requiring that (g_n, h_n) have nontrivial solutions, the dispersion relation is determined from

$$\mathrm{Det}(\boldsymbol{S}\cdot\boldsymbol{U}\cdot\boldsymbol{B} - \boldsymbol{D}\cdot\boldsymbol{V}\cdot\boldsymbol{T}) = 0 \tag{13}$$

where $\boldsymbol{S}$, $\boldsymbol{U}$, $\boldsymbol{B}$, $\boldsymbol{D}$, $\boldsymbol{V}$, and $\boldsymbol{T}$ are matrices with elements $s_{nm}=\alpha_n K_0(\alpha_n a)\delta_{nm}$, $u_{mn}=r_{n-m}$, $b_{nm}=c_{nm}J_1(\beta_{\rho m}a)$, $d_{nm}=K_1(\alpha_n a)\delta_{nm}$, $v_{nm}=w_{n-m}$, and $t_{nm}=c_{nm}\beta_{\rho m}J_0(\beta_{\rho m}a)$.

Generally speaking, a periodic function $\epsilon_r(z)$ possesses all the space harmonic components, indicating that Eq. (13) is the determinant of an infinite-dimensional matrix and needs to be truncated to a finite dimension for numerical evaluation. The convergence of the truncation is guaranteed because the matrix is of Hill's type, and is verified by comparing the results obtained using different orders. If $\epsilon_r(z)$ is of rectangular form as in Eq. (1), $\epsilon'_r(z)$ and $\epsilon''_r(z)$ are singular, making a numerical evaluation difficult. However, in a real physical world there is no ideal step change of $\epsilon_r(z)$; therefore we can approximate $\epsilon_r(z)$ by a finite number of space harmonics and then get the Fourier series of $\epsilon'_r(z)$ and $\epsilon''_r(z)$ from the truncated Fourier series of $\epsilon_r(z)$. In this paper calculations with up to order of ±20 of the Fourier coefficients of $\epsilon_r(z)$ and $\epsilon_r^{\pm 1/2}(z)$ are carried out. There is no real-valued k_{z0} when k_0 falls in the band gap where evanescent modes exist, and k_{z0} should be replaced by the complex wave number $k_{z0}+i\alpha_{z0}$ where α_{z0} and k_{z0} are both real.

A typical dispersion diagram of a PMENGCW is shown in Fig. 2 for which $\epsilon_{ra}=-3.0$ and $\epsilon_{rm}=0.3$ ($\Lambda=10\%$). The dashed line is the dispersion relation of a PMENGCW while the solid line is an ordinary waveguide (no modulation) of $\epsilon_{ra}=-3.0$. The modulation period d for the PMENGCW is chosen to be equal to $\lambda_g/2$ of the nonmodulated waveguide at $k_0a=0.5$. As expected, a band gap appears for the modulated waveguide when k_0a is close to 0.5. Inside the band gap, as expected there is no propagating guided mode, but an evanescent mode exists. The decay constant is also shown in the same plot.

We are actually more interested in the evanescent mode for the purpose of introducing defect into such a waveguide, and here we study the influence of the waveguide parameters on the dispersion properties of the evanescent modes of a PWENGCW. These parameters include (i) the modulation period d; (ii) the relative modulation magnitude $\Lambda = |\epsilon_{rm}/\epsilon_{ra}|$, and (iii) the value of ϵ_{ra}. It is obvious that when all other parameters are fixed but d changes, the operating frequency k_0a will fall into the band gap only when d is in a certain range around $\lambda_g/2$ of the nonmodulated waveguide, and the normalized evanescent constant is maximized when d is properly chosen so that k_0a is close to the center of the band gap, as shown in Fig. 3(a) where $\alpha_z\lambda_0$ is plotted vs $\pi a/d$ for different k_0a. It is interesting to point out that as k_0a decreases, the maximum of $\alpha_z\lambda_0$ increases dramatically, indicating a much sharper decay or much smaller decay distance for small waveguide radius. We are also interested in the influence of Λ and ϵ_{ra} on the band gap width because the band gap is closely connected to the decay constant of the evanescent mode, and usually the bigger the band gap, the

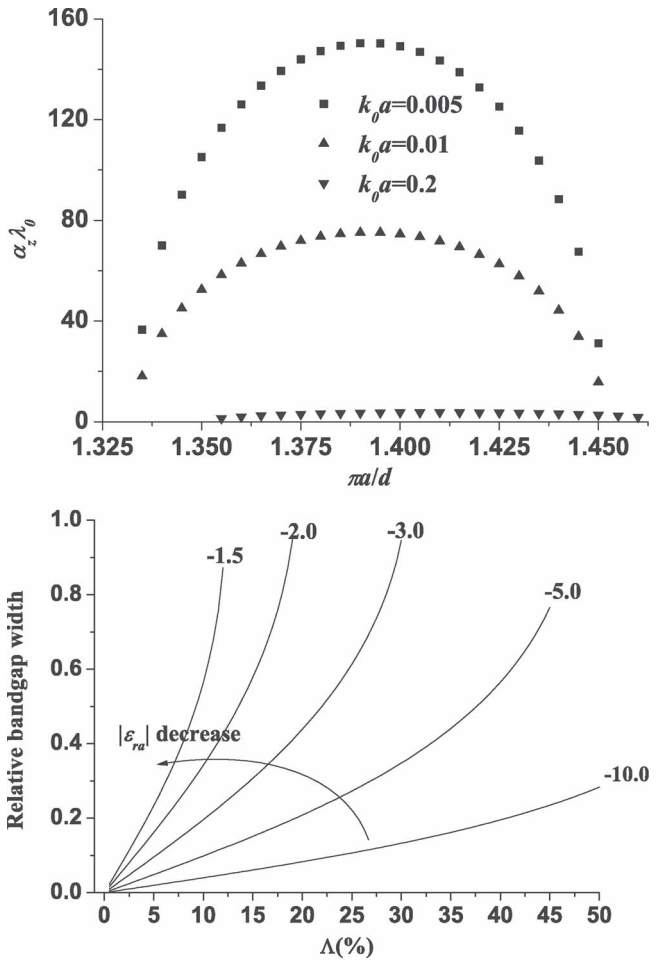

FIG. 3. (a), Normalized decay constant vs modulation period d, $\epsilon_{ra}=-1.5$. (b) Relative band gap width vs Λ. For each ϵ_{ra}, d is chosen as $\lambda_g/2$ of $k_0a=0.5$ when $\Lambda=0$. Here the lossless condition is assumed.

higher the decay constant that can be achieved. The influence of Λ on the band gap is obvious; the band gap width increases as Λ increases, as shown in Fig. 3(b). The normalized band gap width is defined as the width of the band gap divided by $k_0a|_{\Lambda=0}$ and in this plot d is chosen as $\lambda_g/2$ of $k_0a=0.5$ when $\Lambda=0$. It is interesting to point out that for a given Λ, the relative band gap width increases dramatically as $|\epsilon_{ra}|$ decreases. This corresponds to the fact in Fig. 1 that the dispersion relation is much more sensitive to the change of ϵ_{ra} at smaller $|\epsilon_{ra}|$.

IV. DEEP SUBWAVELENGTH CAVITY RESONATOR AND ITS QUALITY FACTOR

A. Cavity resonator of deep subwavelength size on a PMENGCW

With the dispersion relations of the PMENGCW analyzed, we are ready to introduce a defect mode into such a device. In a traditional PC a defect is formed by changing the size or material of one unit cell. Here we would like to introduce it by a conceptual setup. Consider an ordinary ENGCW (no material modulation) connected to a PMENGCW of the same radius. A guided mode with guided wavelength λ_g is launched in the ordinary ENGCW, propagating toward the PMENGCW. The wave is reflected back from the interface between the ENGCW and PMENGCW, forming a standing wave. If the frequency is properly chosen such that k_0a falls into the band gap of the PMENGCW, the field inside the periodic region will be evanescent and all the energy will be bounced back (with some radiation loss, of course, which will be addressed later). Now, considering another PMENGCW put on the same nanowire but approximately $0.5\lambda_g$ away from the former interface, the guided wave between the two PMENGCWs will continuously bounce back and forth. When the length of the ordinary ENGCW inside the two PMENGCWs is properly adjusted so that the standing-wave condition is satisfied, a stable resonating mode is formed. Effectively, it can be viewed as a PMENGCW with a "defect" in it. Actually, the ordinary ENGCW and PMENGCW can be treated as two "effective media" whose dispersion relations are those discussed in Secs. I and II, and for frequencies inside the band gap the PMENGCW medium does not support a propagating mode. A resonating mode can be established when the ordinary ENGCW medium is sandwiched between the PMENGCW media with the length satisfying the resonating conditions. Since the ENGCW can have large k_z (i.e., small λ_g) when the radius decreases to a small value, and at small radius the PMENGCW part can achieve a very high decay rate (Fig. 3), a defect mode formed in this way can have very small dimensions.

Since the form of such a defect mode is longer in the axial direction than in the radial direction, we use the axial length of the mode as a measure for the compactness of this cavity. Inside the PMENGCW the field decays evanescently from the interface with a decay constant α_z; thus the defect mode in each side of the PMENGCW has an effective length of $1/\alpha_z$. The length of the defect part between the two interfaces is determined by the resonating condition which is related to the guided wavelength λ_g and the phase at the interfaces. When the decay in PMENGCW is maximized, the phase shift of the magnetic field at the reflecting interface is close to 0 or close to π (with numerical proofs in the next section); in either case the defect length satisfying the resonating condition is very close to $\lambda_g/2$. We take $\lambda_g/2$ as a good approximation for the mode length between the two PMENGCW interfaces. Considering all this, the effective length of the resonating mode can be defined as

$$L_{\text{eff}} = \frac{\lambda_g}{2} + \frac{2}{\alpha_z}. \tag{14}$$

For a given radius k_0a, the modulation period d can be chosen so that k_0a falls into the band gap and the evanescent decay constant is maximized, as indicated by Fig. 3(a). Since λ_g decreases while the maximum possible α_z increases dramatically as k_0a decreases, L_{eff} is expected to have a very small value at small k_0a. The numerical results are shown in Fig. 4. In these curves we always use for the defect part a material of $\epsilon_r=\epsilon_{ra}$. Curve a is for a waveguide with $\epsilon_{ra}=-1.5$, $\epsilon_{rm}=0.15$ ($\Lambda=10\%$). As we expected, L_{eff} de-

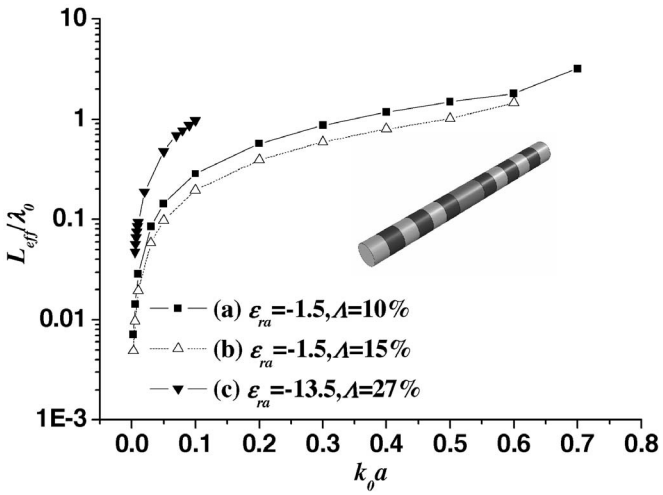

FIG. 4. Effective length of cavity mode on PMENGCW. Inset: 3D model of the cavity.

creases as a decreases, and get below λ_0 when a is smaller than $0.064\lambda_0$. At small normalized radius, L_{eff} decreases almost linearly with decreasing a. When $k_0a=2.5\times10^{-3}$ or $a=4\times10^{-4}\lambda_0$, L_{eff} gets to a value of $7.1\times10^{-3}\lambda_0$, far less than the typical resonating mode dimension of λ_0/n for ordinary dielectrics.

Curves under different conditions are also shown in Fig. 4. At higher relative modulation Λ, L_{eff} achieves an even smaller value for the same radius. Curve b is for $\epsilon_{ra}=-1.50$, $\epsilon_{rm}=0.225$ ($\Lambda=15\%$). For this magnitude of modulation, $L_{\text{eff}}=4.8\times10^{-3}$ when $k_0a=2.5\times10^{-3}$ ($a=4\times10^{-4}$). Curve c is a plot for $\epsilon_{ra}=-13.5$ and $\Lambda=27\%$, Or, $\epsilon_{r\ \text{high}}=-17.15$ and $\epsilon_{r\ \text{low}}=-9.86$. This curve is plotted here because $\epsilon_{r\ \text{high}}$ and $\epsilon_{r\ \text{low}}$ correspond to gold and silver, respectively, for wavelength of 650 nm (with loss neglected). As discussed earlier, the same magnitude of Λ will result in a smaller α_z for bigger $|\epsilon_{ra}|$ [Fig. 3(b)] and thus a bigger L_{eff} for bigger $|\epsilon_{ra}|$. This is verified in Fig. 4 as the curve c is above the other two curves even though it has $\Lambda=27\%$. However, such cavity resonators made of gold and silver will still reach a value of L_{eff} as small as $0.095\lambda_0$ when $k_0a=0.01$ ($a=0.0016\lambda_0$).

B. Quality factor of the cavity resonator

According to Chu's theorem,[24] for a resonating structure, the lower limit of the quality factor (Q) when only radiation loss is considered is proportional to $1/(k_0a)^3$. Here k_0 is the free-space wave number and a is the dimension of the resonating structure. Since the size of the defect mode described here can achieve a very small value, Q is expected to be very high. This can also be understood intuitively. In fact, at the small-radius limit (small k_0a) where small λ_g is achieved, the mode is bound very tightly to the surface. Thus the coupling from the slow, tightly bound propagating mode to the radiation mode at the ENGCW/PMENGCW interface is very weak. This fact is examined by FEM simulations later, which confirm that at the ENGCW/PMENGCW interface the radiation loss is below $\sim10^{-6}$ of the incident power when the frequency is close to the center of the band gap and when the waveguide radius decreases to $\sim0.1\lambda_0$. The loss can be reduced further as the waveguide radius goes down more. Detailed numerical results are given in the next section.

However, it is well known that plasmonic materials have some loss at the frequency of which the permittivity shows a negative real part. This loss needs to be considered and will lower the Q, which may be desirable for certain applications. Since the radiation loss is small, we believe the key factor in determining Q in our problem is the material loss. For calculation of the electromagnetic energy in a temporally dispersive lossy medium we follow the approach used in Ref. 25, where the electromagnetic EM energy in a dispersive, lossy medium is examined, starting from Poynting's theorem, by treating the dispersive medium as an assembly of damped, noninteracting dipoles. Since the permeability of the material discussed here is always μ_0, the stored magnetic energy density is $\mu_0H^2/2$, and we only need to discuss the expression for the stored electric energy. For the electric energy density one has [Eq. (35) in Ref. 25]

$$w_e=\frac{1}{2}\epsilon_0|\boldsymbol{E}|^2+\frac{1}{2\epsilon_0\omega_{ep}^2}\left(\left|\frac{\partial\boldsymbol{p}}{\partial t}\right|^2+\omega_{e0}^2|\boldsymbol{p}|^2\right) \tag{15}$$

and the Ohmic loss of power density from damping is

$$p_{\sigma e}=\frac{\gamma_e}{\epsilon_0\omega_{ep}^2}\left|\frac{\partial\boldsymbol{p}}{\partial t}\right|^2 \tag{16}$$

where ω_{e0} and ω_{ep} are the resonating and plasmonic angular frequencies of the electric dipole, and γ_e is the damping coefficient. In order to get an expression in terms of the constitutive parameters only, we consider the steady state scenario when the stimulation is a sinusoidal electric field of angular frequency ω. Under this situation the dipole is also sinusoidal of the same frequency with a phase difference ϕ with respect to the electric field, and can be written as

$$p=\epsilon_0|\epsilon_r-1|E_0\cos(\omega t-\phi). \tag{17}$$

Inserting Eq. (17) into Eq. (16) and simplifying using $\epsilon_r=1-\omega_{ep}^2/(\omega^2-\omega_{e0}^2-j\omega\gamma_e)$, we can find the average stored electric energy as

$$\bar{w}_e=\frac{1}{4}\epsilon_0E_0^2+\frac{1}{4}\epsilon_0E_0^2\frac{\omega_{ep}^2(\omega^2+\omega_{e0}^2)}{(\omega^2-\omega_{e0}^2)^2+\omega^2\gamma_e^2} \tag{18}$$

since the real part of ϵ_r is $\epsilon_{r1}=1-\omega_{ep}^2(\omega^2-\omega_{e0}^2)/[(\omega^2-\omega_{e0}^2)^2+(\omega\gamma_e)^2]$, Eq. (18) is further simplified as

$$\bar{w}_e=\frac{1}{4}\epsilon_0E_0^2(2-\epsilon_{r1})+\frac{1}{2}\epsilon_0E_0^2\frac{\omega_{ep}^2\omega_{e0}^2}{(\omega^2-\omega_{e0}^2)^2+\omega^2\gamma_e^2} \tag{19}$$

where ϵ_{r1} is the real part of ϵ_r. Since in many practical scenarios the operating angular frequency ω is far away from the characteristic angular frequency ω_{e0}, we can ignore the second term on the right side of Eq. (19). By doing this, we are underestimating the stored energy and thus underestimating Q. For the Ohmic loss, some simple algebraic steps from Eqs. (16) and (17) give the average dissipated power density of material loss as

$$\bar{p}_{\sigma e} = \frac{1}{2}\omega\epsilon_0\epsilon_{r2}E_0^2 \tag{20}$$

where ϵ_{r2} is the imaginary part of ϵ_r. When the field distribution of a defect mode is found, the stored energy and Ohmic dissipation power can be calculated from the volume integral of (19) (with the second term neglected) and (20). Detailed numerical simulation results are presented in the next section.

Strictly speaking, the existence of the imaginary part of the relative permittivity also has an influence on the shape of the dispersion diagram, especially when the loss is not small. With the relative permittivity taking a complex value, the analytical approach in Sec. II can also deal with lossy materials, but the mathematical process will be much more complicated. In this paper, we use a simplified approach, that is, we get the dispersion relation and the resonant mode by assuming the material is lossless, then we estimate the stored energy from the field distribution achieved under no-loss assumptions, and finally we use the material loss to estimate Q. Both analytical and FEM simulation take this simplified approach. With this approach the physical meaning of the problem can be more easily understood.

V. FINITE-ELEMENT METHOD SIMULATION

A. Reflection from ENGCW/PMENGCW interface

FEMLAB is used to demonstrate this cavity resonator. Reflection at the ENGCW/PMENGCW interface is first studied, with the three-dimensional (3D) plot of the structure in Fig. 5(b). A piece of ordinary ENGCW of radius a serving as a "feeding" waveguide is connected to one end of a PMENGCW of the same radius. Since the mode has no angular variation, an azimuthally symmetric 2D model corresponding to the cross section from $r=0$ to $10a$ is used [the top plot of Fig. 5(a)]. The absorbing boundary condition is applied at the side boundary. At the input end of the feeding waveguide, a stimulating field with the magnitude distribution corresponding to the form of the guided mode is applied. This will launch a propagating guided mode in the feeding waveguide, which reflects at the interface. The parameters used here are, for the feeding waveguide, $\epsilon_r=-1.5$, while for the PMENGCW, $|\epsilon_{ra}|=-1.5$ and $\epsilon_{rm}=0.15$ (or $\epsilon_{r\ \mathrm{low}}=-1.35$ and $\epsilon_{r\ \mathrm{high}}=-1.65$). The frequency was chosen such that $k_0a=0.005$, and $d/a=1.13$ is used, which provides the highest α_z according to the analytical result in Sec. III. The second plot of Fig. 5(a) shows the simulation result of the magnitude of the magnetic field. It can be clearly seen that, inside the PMENGCW, the magnitude of the field decays very quickly from the ENGCW/PMENGCW interface. Figure 5(c) is the magnitude of H_ϕ in the PMENGCW extracted from the FEM result, and the dashed line is an exponentially decaying fitted curve using the decay constant obtained from the analytical approach discussed in Sec. II. As can be seen, there is an excellent match between the two results. The radiation loss at the reflection can be examined by a numerical integration of power flow through the side boundaries. The result shows that only about $\sim 10^{-7}$ of the incident power is radiated away from the waveguide. The low-

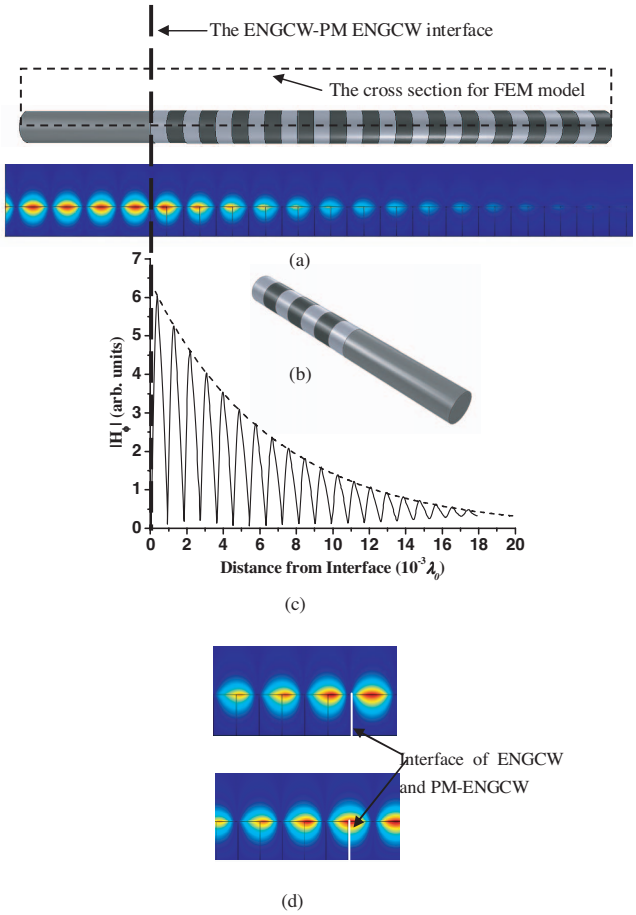

FIG. 5. (Color online) FEM demonstration of reflection from ENGCW/PMENGCW interface. (a), The horizontal view of the model (top), and the FEM result for the magnitude of the magnetic field (bottom). (b) 3D plot of the model. (c) Distribution of the magnetic field magnitude inside PMENGCW extracted from FEM results. Dashed line, $1/\alpha_z$ with α_z obtained from the analytical approach in Sec. II. (d) Reflection from PMENGCW with the material of the first half period different. Top: $\epsilon_{r\ \mathrm{low}}$. Bottom: $\epsilon_{r\ \mathrm{high}}$. The interface is highlighted. Lossless materials are assumed here.

radiation-loss feature can also be examined by the field distribution in front of the interface where a standing wave with the minimum going almost to zero is formed. A high-magnitude standing-wave ratio indicates that the magnitude of the reflection coefficient is almost 1, implying that a very small fraction of energy has been radiated away.

A careful examination of the problem shows that there can be two ways of forming the interface. We can use either $\epsilon_{r\ \mathrm{low}}$ or $\epsilon_{r\ \mathrm{high}}$ for the first half period of the PMENGCW right after the feeding waveguide. From the point of view of the decay constant, the two cases are equivalent, since the PMENGCW side forms the same "effective medium." The differences are at the interface. When $\epsilon_{r\ \mathrm{low}}$ is used for the first half period, H_ϕ is near zero at the interface, indicating a phase close to π at the reflection; while for the case of $\epsilon_{r\ \mathrm{high}}$, the magnitude at the interface is close to maximum, indicating an almost zero phase for the reflection [see Fig. 5(d)]. These details have an important influence on the shape of the defect mode.

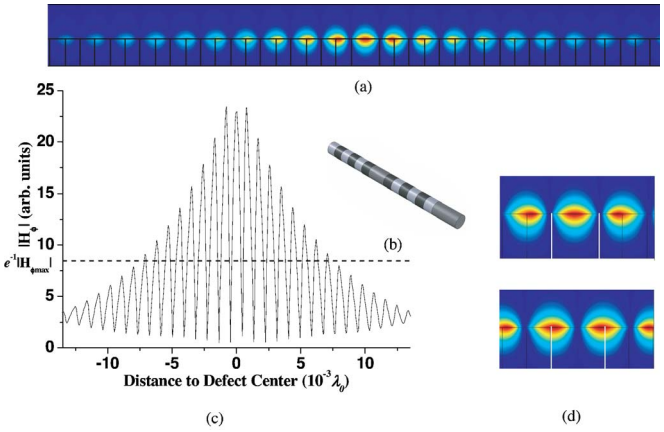

FIG. 6. (Color online) FEM simulation of cavity resonator on PMENGCW. (a) Plot of FEM result for $|H_\phi|$. The brightest part in the center is the position of the cavity. (b) 3D model of the device. (c) The distribution of $|H_\phi|$ of the cavity mode extracted from FEM results. (d) Two types of cavity mode: Top: π mode. Bottom: 0 mode. Lossless materials are assumed here.

B. Numerical simulation of the deep subwavelength cavity resonator

The method that is used here to simulate the cavity mode on the PMENGCW is similar to the conventional finite-difference time-domain (FDTD) or plane-wave approach for PCs, where the defect mode is studied by finding the dispersion diagram of a "superunit" composed of several PC periods with a defect in the middle and with appropriate periodic boundary conditions. The model used here is shown in Fig. 6(b). A defect is formed by sandwiching a piece of the ENGCW of length $\sim\lambda_g/2$ in between two PMENGCWs of enough periods, and another piece of ENGCW is connected at one end serving as the feeding waveguide. Stimulation is applied at the input of the feed. The mode is very sensitive to the defect length, and therefore the length of the defect should be carefully adjusted around $\lambda_g/2$ so that the resonating conditions are satisfied. At the interface between the feeding part and the first PMENGCW, a reflection of ~ 1 happens with the field decaying evanescently into the PMENGCW. However, the field will "leak" into the defect, and when the length of the defect satisfies the resonating condition, a resonating mode with magnitude much higher than the input will build up. The magnitude of the magnetic field distribution for such a resonator is shown in Fig. 6(a) and 6(c) is the plot of the field magnitude vs position extracted from the FEM simulation. Parameters used here are $k_0a=0.005$ (or $a=8\times10^{-4}\lambda_0$); for the PMENGCW $\epsilon_{ra}=-1.5$ and $\epsilon_{rm}=0.15$, while for the defect and feeding parts, $\epsilon_r=-1.5$. Twenty periods of the PMENGCW are used at both sides of the defect, but in Fig. 6(a) only the defect and several adjacent periods are shown. A zoomed-in plot of Fig. 6(a) can be found as the top plot in Fig. 6(d). The defect mode is obviously stimulated and has a much higher magnitude than the incident field, which is expected in a typical resonating phenomenon. The equivalent mode length can also be evaluated from the field magnitude vs position plot in Fig. 6(c) by finding the position where $|H_\phi|$ is equal to $|H_\phi|_{\max}/e$. For the parameters used here the mode length is approximately $0.015\lambda_0$, close to the value of $0.0142\lambda_0$ that we obtained by the analytical approach. Cases with different diameters are simulated, with the results being compared with the analytical results in Table I. The two results match well.

As can be seen in Fig. 5(d), choosing a different material ($\epsilon_{r\ \mathrm{low}}$ or $\epsilon_{r\ \mathrm{high}}$) for the first half period right next to the defect will result in a different phase at the interface. In the $\epsilon_{r\ \mathrm{low}}$ case, the phase is close to π, while in the $\epsilon_{r\ \mathrm{high}}$ case, it is close to 0. It is easy to determine that this will have little influence on the defect length required for the resonating condition and in both cases, the proper defect length is close to $\lambda_g/2$. However, it will have an obvious influence on the shape of the mode. In the $\epsilon_{r\ \mathrm{low}}$ case, the maximum of the magnetic field happens at the center of the defect; while in the $\epsilon_{r\ \mathrm{high}}$ case, the situation is reversed, where the magnetic field is maximum around the interfaces. Figure 6(d) gives a zoomed-in picture of the defect mode for the two different cases. The difference of the maximum position of the magnetic field is obvious. We call the first one a "π" mode and the second one a "0" mode.

In the context of PCs, the volume of a defect mode is often defined as[18]

$$V=\frac{\int \epsilon E^2(\boldsymbol{r})d\boldsymbol{r}^3}{[\epsilon E^2(\boldsymbol{r})]_{\max}} \tag{21}$$

and for different forms of cavities the smallest mode volume is approximately $(\lambda_0/n)^3$. For the sake of comparison, the

TABLE I. Properties of defect mode for $\epsilon_{ra}=-1.5$, $\epsilon_{rm}=0.15$. "Analytical" denotes the effective mode lengths evaluated from the analytical approach, while "FEM" refers to those obtained by the FEM simulation. Q is the value for $\gamma=0.01$ (see Sec. VI).

	$L_{\mathrm{eff}}(\lambda_0)$				
$k_0a(\lambda_0)$	Analytical	FEM	Q	$V(\lambda_0^3)$	$Q/V(\lambda_0^{-3})$
0.0025	0.00712	0.0073	169.2	2.4×10^{-10}	7.20×10^{11}
0.005	0.0142	0.015	169.1	1.9×10^{-9}	3.57×10^{11}
0.01	0.0285	0.029	169.2	1.5×10^{-8}	1.13×10^{10}
0.05	0.142	0.15	169.2	1.9×10^{-6}	8.90×10^{8}
0.1	0.285	0.29	169.2	1.5×10^{-5}	1.13×10^{7}
0.5	1.482	1.52	170.6	1.8×10^{-3}	9.50×10^{4}

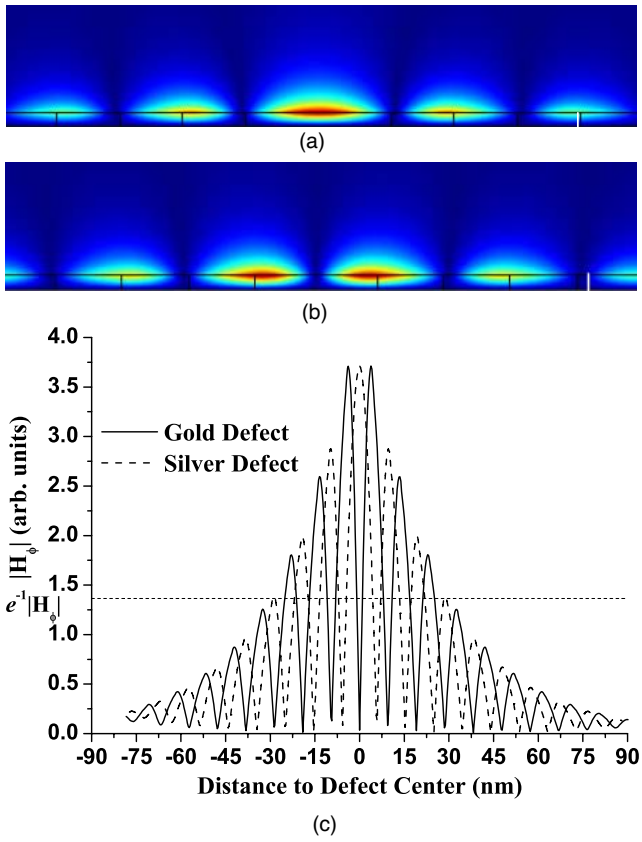

FIG. 7. (Color online) (a) FEM simulation of Ag defect in Au/Ag PMENGCW. (b) FEM simulation of Au defect in Au/Ag PMENGCW. (c) Distribution of magnetic field magnitude extracted from the FEM simulations.

mode volume for our cavity resonator is also calculated here. Since in our case negative ϵ_r are used, Eq. (21) cannot be applied directly here. Noticing the fact that the numerator of Eq. (21) is the total stored electric energy of the defect mode while the denominator is the maximum electric energy density, we rephrase the definition in order to address the presence of negative ϵ_r as

$$V = \frac{\int w_e d\boldsymbol{r}^3}{w_e|_{\max}} \tag{22}$$

where $w_e = \epsilon_0(2-\varepsilon_r)E^2/4$ from Eq. (19) for negative ϵ_r and $w_e = \epsilon_0 E^2/4$ for free space. As expected, since the cross section of the mode is even much smaller than the length of the mode, we have a mode volume much smaller than the conventional value. For example, for $k_0a = 2.5\times10^{-3}$ ($a = 4\times10^{-4}\lambda_0$) the mode volume is $V = 2.34\times10^{-10}\lambda_0^3$, far less than the value of $(\lambda_0/n)^3$ in ordinary PCs. Mode volumes for different k_0a are shown in Table 1.

Finally, the simulation result for a cavity resonator realized on nanowires made of gold and silver, the two most commonly used plasmonic materials, is shown in Fig. 7. At a wavelength of 650 nm, for gold we have $\epsilon_r = -9.86 + 1.046i$ and for silver $\epsilon_r = -17.20 + 1.162i$.[26] However, for the moment, in these simulations the imaginary parts of permittivities are ignored (see the next section for discussion on material loss). In previous discussions we used a plasmonic material with $\epsilon_r = \epsilon_{ra}$ for the defect. However, in general this would not be necessary. We can use any plasmonic material for the defect part (also the feeding part) only if the length of the defect is well adjusted so that the resonating conditions are satisfied for this specific material. It would be more convenient from a potential experimental point of view to have the defect made of one of the materials for the modulated part, so that the whole process will have only two materials involved. Figure 7 shows the simulation results for cavities made of gold and silver (with zero imaginary parts of the permittivities) with $k_0a = 0.01$ ($a = 0.0016\lambda_0$). In Fig. 7(a), silver is the material of the defect (silver defect) while in Fig. 7(b) gold is used for the defect (gold defect). Figure 7(c) is the magnitude of the magnetic field extracted from the FEM simulation. Since silver has a higher magnitude of ϵ_r, the π mode is expected for the silver defect and the 0 mode for the gold defect, as can be seen in the figure.

VI. DISCUSSION

A. Effects of material loss

In our calculations and simulations described above, for the sake of simplicity we assumed that the material was lossless. However, in most cases the material losses of plasmonic materials such as noble metals cannot be neglected. Therefore, even though the radiation loss is very small when k_0a is small as discussed before, the quality factor can be low due to the material loss. We can estimate the quality factor from the FEM result. The stored electrical energy $\bar{W}_e$ is evaluated by a numerical volume integration of the first term in the right side of Eq. (19), and the stored magnetic energy $\bar{W}_h$ is easily obtained from the volume integration of $\mu_0|H|^2/2$. Since the cavity mode is a TM (or p-polarized) mode, $\bar{W}_e \gg \bar{W}_h$. Q is then effectively evaluated as $Q = \omega\bar{W}_e/P_{\sigma e}$, where $P_{\sigma e}$ is the volume integration of material loss power density as in Eq. (20). The numerical result for Q depends on the specific material parameters used. For the sake of a simple estimation we assume the ratio of the imaginary part of the permittivity to its real part to be γ for all materials involved ($\epsilon_{r\,\mathrm{low}}$, $\epsilon_{r\,\mathrm{high}}$, and ϵ_r of the defect). For the cavity mode in Fig. 6, when the radius gets as small as $k_0a = 0.0025$ (or $a = 4\times10^{-4}\lambda_0$) we get $Q = 1.69/\gamma$ for the π mode (the 0 mode has similar results). For example, for $\gamma = 0.01$, $Q = 169$. Q is almost the same for a wide range of radius. For k_0a ranging from 0.5 to 0.0025 (or $a = 8\times10^{-2} - a = 4\times10^{-4}$), Q is in the range of 169 to 171 for $\gamma = 0.01$. The quality factor is mainly determined by the material loss. This is different from most of the previous studies of PC cavities with positive-permittivity dielectrics (with essentially no material loss) where radiation loss is assumed to be the main mechanism for energy dissipation.[18,19]

Compared to that of a high-Q PC cavity whose quality factor can be as high as 10^6, the Q values we achieved here are much smaller, simply because material loss is taken into account and the loss is relatively high for plasmonic materials. However, in many situations the figure of merit for cav-

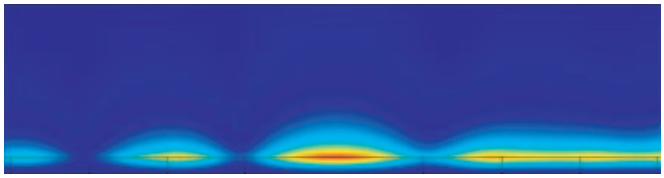

FIG. 8. (Color online) FEM simulation of Ag defect in Au/Ag PMENGCW with real material loss considered. $k_0a=0.01$ ($a=0.0016\lambda_0$) at wavelength 650 nm. Because of the material loss, the right side of the cavity has a higher magnitude to the left side (the stimulation begins from the right.)

ity design can be Q/V, where V is the mode volume.[18] Since the mode volume in our geometry is very small as discussed above, Q/V can still achieve a high value. As an example, for $a=4\times10^{-4}\lambda_0$, $\epsilon_{ra}=-1.5$, $\epsilon_{rm}=0.15$, and $\gamma=0.01$, we have $Q=169$, $V=2.34\times10^{-10}\lambda_0^3$ so that $Q/V=7.2\times10^{11}\lambda_0^{-3}$, much higher than $n^3\times10^6\lambda_0^{-3}$ for a PC cavity realized using ordinary dielectrics. A detailed list of simulation results for different radius can be found in Table I. The Q and Q/V for cavity modes on gold and silver devices in Fig. 7 can also be estimated. For the silver defect we have $Q=11.6$ but $Q/V=2.66\times10^8\lambda_0^{-3}$, while for the gold defect $Q=8.3$ and $Q/V=7.00\times10^7\lambda_0^{-3}$.

Since for many plasmonic materials loss is present, we also need to estimate the decay constant due to the material loss. This decay length increases with the imaginary part of the permittivity but should be no more than the decay caused by the permittivity modulation in order to achieve a good cavity mode. For an ENGCW with the real part of the permittivity $\epsilon_{r1}=-1.5$, the decay constant due to the material loss increases almost linearly with the magnitude of the imaginary part of the permittivity when the radius is small. For $k_0a=0.005$ and for γ being 0.01 and 0.02 the normalized decay constant $\alpha_z\lambda_0$ is 72.5 and 144.5, respectively. Thus for the PMENGCW considered in Fig. 3 to work properly, the magnitude of the imaginary part of the permittivity should be no more than 2% of its real part for these specific design parameters. Careful design is required if the material loss is higher than this limit. For example, using plasmonic materials of higher permittivity contrast can provide greater modulation, which leads to higher decay constant due to permittivity modulation. Materials of higher magnitude (negative) permittivity will also decrease the influence of the material loss on the mode shape. For example, Fig. 8 shows the simulation result of the cavity mode on a nanowire made of gold and silver (silver defect) with $k_0a=0.01$ at 650 nm. Even though $\gamma=0.11$ for gold and $\gamma=0.07$ for silver, the cavity mode is still obviously stimulated. (Although the wire radius chosen in this simulation is quite small, the simulation reveals the effects under discussion. In Sec. VI C, we briefly discuss the issue of limits for small radii.)

B. Achieving permittivity modulation

In order to fabricate the cavity resonator described above, at least two types of plasmonic materials whose permittivities are different at the operating frequency are desired. The noble metals are commonly used for visible wavelengths. If

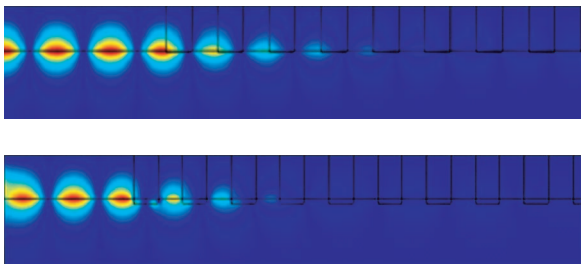

FIG. 9. (Color online) FEM simulation of reflection from interface between ENGCW and periodically corrugated ENGCW. $\epsilon_r=-1.5$, $k_0a=5\times10^{-3}$. Corrugation height (a) $2\%a$ and (b): $10\%a$.

one is interested in a wide range of wavelengths from ultraviolet to far infrared, many candidate materials can be found. These include, but are not limited to, lithium, sodium, and magnesium in the 320–600 nm range; lithium and sodium in the 320–800 nm range; sodium nitrate and calcium carbide in the 6.97–7.20 μm range, silicon carbide and beryllium oxide in the 10.64–12.20 μm range, etc.[26] A discussion of the conditions and possibilities of integrating and fabricating two or three of these materials together in order to form a PMENGCW is not within the subject of the paper. Here we are listing these materials as possible candidates.

Another way of forming the PMENGCW using only one material is by spatially (and periodically) varying the diameter of the nanowire instead of the permittivity. There have been a lot of studies dealing with periodical modulation of the diameter of cylindrical structures, mostly in the radio frequency (RF) regime and used for leaky wave antennas (see, for example, Ref. 27). By applying a mathematical approach similar to the one presented here that problem can also be solved rigorously. Rather than introducing another mathematical process here, we explain it intuitively with the concept of the effective dielectric constant (EDC). Considering an ENGCW whose radius is modulated periodically between a_1 and a_2. From Fig. 1 we can see that waves propagated along the two segments of different radii will have different guided propagation constants. From the EDC point of view, such a difference in guided propagation constant can be viewed effectively as a difference in permittivity of segments with the same radius. Figure 1 also shows that, when the radius is small, a very tiny variation in radius can cause a noticeable change in the guided propagation constant, which means an efficient modulation of the effective dielectric constant. Strictly speaking, each half period here is only $\sim\lambda_g/4$ of that material; thus the application of the EDC concept is not necessarily rigorous, but it is adequate for a preliminary description. Figure 9 shows the simulation of the reflection at the interface of a corrugated ENGCW. The material used has $k_0a=0.005$ and the corrugation height is 2% of the radius for Fig. 9(a) and 10% for Fig. 9(b). It is obvious from the simulation result that at this radius a diameter variation as small as 2% already provides very good decay constants, and for higher corrugation the decay is even stronger. The normalized radiation loss still remains as low as $\sim10^{-7}$. Because the structure has a lot of sharp corners, a huge mesh density is required for the FEM simulation to converge, making the simulation very time consuming.

In the discussions above we focused on plasmonic materials in the optical domain. There have been a lot of discussions of metamaterials in the RF and microwaves regimes, providing the possibilities for theoretical and experimental techniques to achieve artificial materials with negative permittivity and/or negative permeability. Situations of periodic modulated μ-negative cylindrical waveguides can also be studied using a similar algorithm. With the possibility of engineering desired values of constitutive parameters in artificial materials and metamaterials, achieving deep subwavelength resonating cavities in the RF and microwave regimes can also provide exciting potential applications.

C. Lower limit for wire diameter

Following the previous discussions, a question may arise naturally: What will happen if we continuously decrease the diameter of the cavity resonator? The theory provided here does not predict a lower limit to the mode length. However, when the diameter is small and comparable to the atomic lattice size of the material, bulk material parameters such as permittivity have no meaning. In this case, the quantum effects should be taken into account. For some of the cases provided above this would not be a problem. For example, if we use silicon carbide at 10.65 μm wavelength for $\epsilon_r = -1.5$, $\Lambda = 10\%$, and realize the effective permittivity modulation using the periodical radial modulation, at $k_0 a = 0.005$ the diameter of the waveguide is $\sim$17 nm, good enough to still use a bulk description. For these parameters, we can achieve an effective mode length of $\sim 0.014\lambda_0$, only $\sim$150 nm. However, both gold and silver have a face centered cubic structure with a lattice constant of $\sim$0.4 nm, which means the distance between each two atoms is about 0.283 nm. At a wavelength of 650 nm for a cavity resonator of $k_0 a = 0.01$, as we simulated before, it has a cylindrical structure of diameter 2.07 nm. At this dimension, bulk descriptions of material properties may not be adequate. If we choose $\sim$10 nm as the critical dimension where the bulk description may still be effective, it will correspond to $k_0 a = 0.05$ for the gold or silver structure and the smallest mode length we can achieve will be $\sim 0.465\lambda_0$. This is mainly because an ENGCW with $|\epsilon_r|$ much bigger than unity will have relatively bigger λ_g at the same radius. Moreover, for the same modulation magnitude Λ, those $|\epsilon_{ra}|$ much bigger than unity will provide a smaller decay rate when operated in the band gap (Fig. 3). However, this does not necessarily imply that it would be impossible to get a deep subwavelength cavity at optical wavelengths using gold and silver. If these cavities made of gold and silver are embedded in a host medium with a positive permittivity close to the magnitude of the permittivity of gold or silver, the band structure of such a device will be similar to that of $\epsilon_{r\,\mathrm{low}} = \epsilon_{r\,\mathrm{gold}}/\epsilon_{r\,\mathrm{host}}$ and $\epsilon_{r\,\mathrm{high}} = \epsilon_{r\,\mathrm{silver}}/\epsilon_{r\,\mathrm{host}}$, much closer to -1. In such cases, one may anticipate that a higher decay rate in the band gap will be possible, leading to a small mode length at a relatively bigger diameter. Of course, in this situation the equivalent λ_0 also becomes smaller ($\lambda_0/\sqrt{\epsilon_{r\,\mathrm{host}}}$) and the 10 nm critical diameter corresponds to $k_0 a = 0.05 \times \sqrt{\epsilon_{r\,\mathrm{host}}}$. With this compromise we may still expect that this method can achieve small mode length for high-magnitude negative-permittivity materials.

VII. CONCLUSIONS

In this work we suggested a way of achieving a deep subwavelength cavity resonator exploiting the features of small guided wavelength of an ϵ-negative cylindrical waveguide. By sandwiching a small segment of ENGCW between cylindrical photonic crystals realized by periodically modulating the permittivity of the ENGCW and operating at the frequency inside the band gap, an ultracompact resonating mode can be established. FEM simulations were used to demonstrate the cavity mode and the quality factors were calculated numerically. We believe such a way of realizing a small size-resonator is of interest in the design of nanoscale devices in the optical domain.

ACKNOWLEDGMENTS

This work is supported in part by the U.S. Air Force Office of Scientific Research (AFOSR) Grant No. FA9550-05-1-0442.

*Electronic address: jingjing@seas.upenn.edu
†Electronic address: engheta@ee.upenn.edu

[1] S. A. Maier and H. A. Atwater, J. Appl. Phys. **98**, 011101 (2005).
[2] T. W. Ebbsen, H. J. Lezec, H. F. Ghaemi, T. Thio, and P. A. Wolff, Nature (London) **391**, 667 (1998).
[3] D. E. Grupp, H. J. Lezec, T. Thio, and T. W. Ebbesen, Adv. Mater. (Weinheim, Ger.) **1**, 860 (1999).
[4] G. Schider, J. R. Krenn, A. Hohenau, H. Ditlbacher, A. Leitner, F. R. Aussenegg, W. L. Schaich, I. Puscasu, B. Monacelli, and G. Boreman, Phys. Rev. B **68**, 155427 (2003).
[5] W. L. Barnes, A. Dereux, and T. W. Ebbesen, Nature (London) **424**, 824 (2003).
[6] L. A. Sweatlock, S. A. Maier, H. A. Atwater, J. J. Penninkhof, and A. Polman, Phys. Rev. B **71**, 235408 (2005).
[7] J. Takahara, S. Yamagishi, H. Taki, A. Morimoto, and T. Kobayashi, Opt. Lett. **22**, 475 (1997).
[8] P. Muhlschlegel, H. J. Eisler, O. J. F. Martin, B. Hecht, and D. W. Pohl, Science **308**, 1607 (2005).
[9] N. Fang, H. Lee, C. Sun, and X. Zhang, Science **308**, 534 (2005).
[10] G. Shvets and Y. A. Urzhumov, Phys. Rev. Lett. **93**, 243902 (2004).
[11] H. Ditlbacher, A. Hohenau, D. Wagner, U. Kreibig, M. Rogers, F. Hofer, F. R. Aussenegg, and J. R. Krenn, Phys. Rev. Lett. **95**, 257403 (2005).
[12] N. Engheta, A. Salandrino, and A. Alu, Phys. Rev. Lett. **95**, 095504 (2005).
[13] E. Yablonovitch, Phys. Rev. Lett. **58**, 2059 (1987).
[14] A. S. Barlevy and Y. Rahmat-Samii, IEEE Trans. Antennas

Propag. **49**, 343 (2001).
[15] M. H. Qi, E. Lidorikis, P. T. Rakich, S. G. Johnson, J. D. Joannopoulos, E. P. Ippen, and H. I. Smith, Nature (London) **429**, 583 (2004).
[16] A. Christ, T. Zentgraf, J. Kuhl, S. G. Tikhodeev, N. A. Gippius, and H. Giessen, Phys. Rev. B **70**, 125113 (2004).
[17] G. Shvets and Y. A. Urzhumov, J. Opt. A, Pure Appl. Opt. **7**, S23 (2005).
[18] D. Englund, I. Fushman, and J. Vuckovic, Opt. Express **13**, 5961 (2005).
[19] R. Coccioli, M. Boroditsky, K. W. Kim, Y. Rahmat-Samii, and E. Yablonovitch, IEE Proc.: Optoelectron. **145**, 391 (1998).
[20] A. Alu and N. Engheta, IEEE Trans. Microwave Theory Tech. **52**, 2004 (2004).
[21] N. Engheta, IEEE Antennas Wireless Propag. Lett. **1**, 10 (2002).
[22] A. Alu and N. Engheta, IEEE Trans. Antennas Propag. **51**, 2558 (2003).
[23] S. T. Peng, T. Tamir, and H. L. Bertoni, IEEE Trans. Microwave Theory Tech. **23**, 123 (1975).
[24] J. L. Chu, J. Appl. Phys. **19**, 1163 (1948).
[25] T. J. Cui and J. A. Kong, Phys. Rev. B **70**, 205106 (2004).
[26] *Handbook of Optical Constants of Solids*, 2nd ed., edited by E. D. Palik, Academic Press Handbook Series Vol. 1 (Academic Press, Orland, FL, 1985).
[27] S. T. Peng, S. J. Xu, and F. K. Schwering, in IEEE Antennas and Propagation Society International Symposium (Philadelphia, PA, 1986), Vol. 24, p. 697–700.